Research Article

El Sayed M. Tag El Din, Tanveer Sajid, Wasim Jamshed*, Syed Zahir Hussain Shah, Mohamed R. Eid, Assad Ayub, Kamel Guedri, Manuel Sánchez-Chero, José Antonio Sánchez Chero, Gilberto Carrión Barco, and Gisella Luisa Elena Maquen-Niño

Cross electromagnetic nanofluid flow examination with infinite shear rate viscosity and melting heat through Skan-Falkner wedge

https://doi.org/10.1515/phys-2022-0216
received July 16, 2022; accepted November 21, 2022

Abstract: This demonstration of study focalizes the melting transport and inclined magnetizing effect of cross fluid with infinite shear rate viscosity along the Skan-Falkner wedge. Transport of energy analysis is brought through the melting process and velocity distribution is numerically achieved under the influence of the inclined magnetic dipole effect. Moreover, this study brings out the numerical effect of the process of thermophoresis diffusion and Brownian motion. The infinite shear rate of viscosity model of cross fluid reveals the set of partial differential equations (PDEs). Similarity transformation of variables converts the PDEs system into nonlinear ordinary differential equations (ODEs). Furthermore, a numerical bvp4c process is imposed on these resultant ODEs for the pursuit of a numerical solution. From the debate, it is concluded that melting process cases boost the velocity of fluid and velocity ratio parameter. The augmentation of the minimum value of energy needed to activate or energize the molecules or atoms to activate the chemical reaction boosts the concentricity.

Keywords: inclined magnetized flow, infinite shear rate viscosity, Brownian motion, 2-D cross fluid, melting process of energy, thermophoresis diffusion

*** Corresponding author: Wasim Jamshed,** Department of Mathematics, Capital University of Science and Technology (CUST), Islamabad, 44000, Pakistan, e-mail: wasiktk@hotmail.com
El Sayed M. Tag El Din: Department of Electrical Engineering, Faculty of Engineering and Technology, Future University in Egypt, New Cairo 11835, Egypt
Tanveer Sajid: Department of Mathematics, Capital University of Science and Technology (CUST), Islamabad, 44000, Pakistan
Syed Zahir Hussain Shah, Assad Ayub: Department of Mathematics & Statistics, Hazara University, Mansehra, 21300, Pakistan
Mohamed R. Eid: Department of Mathematics, Faculty of Science, New Valley University, Al-Kharga, Al-Wadi Al-Gadid, 72511 Egypt; Department of Mathematics, Faculty of Science, Northern Border University, Arar, 1321, Saudi Arabia
Kamel Guedri: Mechanical Engineering Department, College of Engineering and Islamic Architecture, Umm Al-Qura University, P. O. Box 5555, Makkah 21955, Saudi Arabia
Manuel Sánchez-Chero, José Antonio Sánchez Chero: Universidad Nacional de Frontera, Sullana, Perú
Gilberto Carrión Barco: Universidad Tecnológica del Perú, Chiclayo, Perú
Gisella Luisa Elena Maquen-Niño: Universidad: Universidad Nacional Pedro Ruiz Gallo, Lambayeque, Perú

Nomenclature

a, b, c, m	positive constants
A	notation of unsteadiness parameter
A_1	first Rivlin (Erickson tensor)
c_f	notation of skin friction
c_p	notation of specific heat of fluid
C	concentration profile
I	notation of identity tensor
k	cross nanofluid thermal conductivity
M	notation of melting parameter
n	notation of power law index region
Nu	notation of Nusselt number
p	exertion of pressure
Pr	notation of Prandtl number
q_w	notation of wall shear stress
Re	notation of Reynold number
k_c	chemical reaction parameter
s	velocity ratio parameter
Sc	notation of Schmidt number
t	time involved in stream function
T	temperature profile
T_0	initial temperature
T_∞	ambient temperature of fluid
T_m	temperature during melting process
$U_e(x, t)$	free stream velocity
$U_w(x, t)$	stretching velocity

u, v	velocity components
V	velocity profile
We	Weissenberg number
$\boldsymbol{x}, \boldsymbol{y}$	space coordinates
β	wedge angle parameter
τ	Cauchy stress tensor
μ_0	zero viscosity in shear rate model
μ_∞	infinite viscosity shear rate model
Γ	notation of relaxation time constant
$\psi(x, y, t)$	Stokes stream function
μ	notation of viscosity
τ_{rx}	heat flux
$\dot{\gamma}$	shear strain of shear rate model
η	involved in stream function dimensionless variable
σ	reaction rate parameter
ρ	density
θ_w	temperature ratio parameter
α_m	notation of thermal diffusivity

1 Introduction

Nanotechnology is defined as the use of nanoparticles for human benefit. Nanomaterials have special properties due to their physical and chemical properties at the nanoscale. Nanotechnology has a wide range of applications and has been used to design new technologies in the manufacturing, electrical, and energy sectors. The modification of matter with at least one dimension sized between 1 and 100 nm is characterized as nanomaterials. Nanofluid and nanoscale surface morphology are two commonly utilized nanotechnologies for boiling heat transfer. The basic process is that nano-products can alter the thermal properties of the heating surface or the base fluid, resulting in improved boiling heat transmission ability. Nanoscale coating primarily affects the wickability, wettability, and porosity of surfaces. The capillary action, which absorbs fresh liquid to dry out patches, can be delayed by modifying the surface wickability. Nanoscience gave a new dimension to heating transfer fluid. Thermal science is facing the consumption of energy, and to overcome this issue, industrial areas needed to increase the thermal conductivity of the base fluid. Nanoscience gave the way to increase the thermal conductivity of heat transfer fluid, and thus, nanoscience has been extensively engaged in industrial and engineering areas because low thermal conductivity was the main problematic issue for engineering framework. Nanoscience introduced nano liquids which are very imperative to increase thermal conductivity. Many scholars [1–4] made their studies related to fluidic models by considering several nanoparticles with base fluid. Investigation of nanoparticles of Maxwell fluid model by taking several nanoparticles distributed over the surface is discussed in detail by Asjad *et al.* [5]. The purpose of enhancement of thermal conductivity with cross nanofluid over wedge geometry is explained by Waqas *et al.* Blood behavior as a cross fluid is achieved numerically taken into consideration the influence of nanoparticles by ref. [6].

The minimum amount of energy required for the possible process of emission or reaction is called activation energy. It activates the chemical process. In engineering point of view, it has a magnificent and vital role like its usage in geothermal reservoirs, emulsion of oil, food processing, water mechanisms, *etc.* several scholars [7,8] made their efforts related to the investigation to judge the concentration of flow with activation energy. The effect of activation energy on the concentration profile

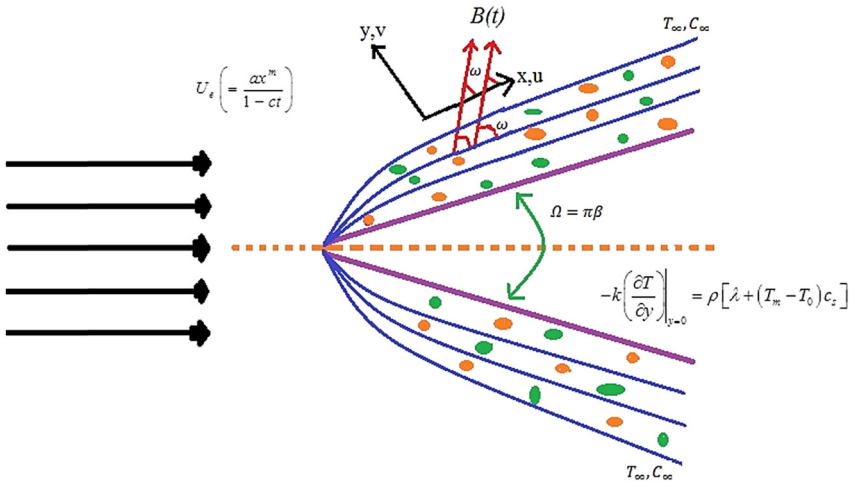

Figure 1: Geometry related to the physical flow of cross nanofluid.

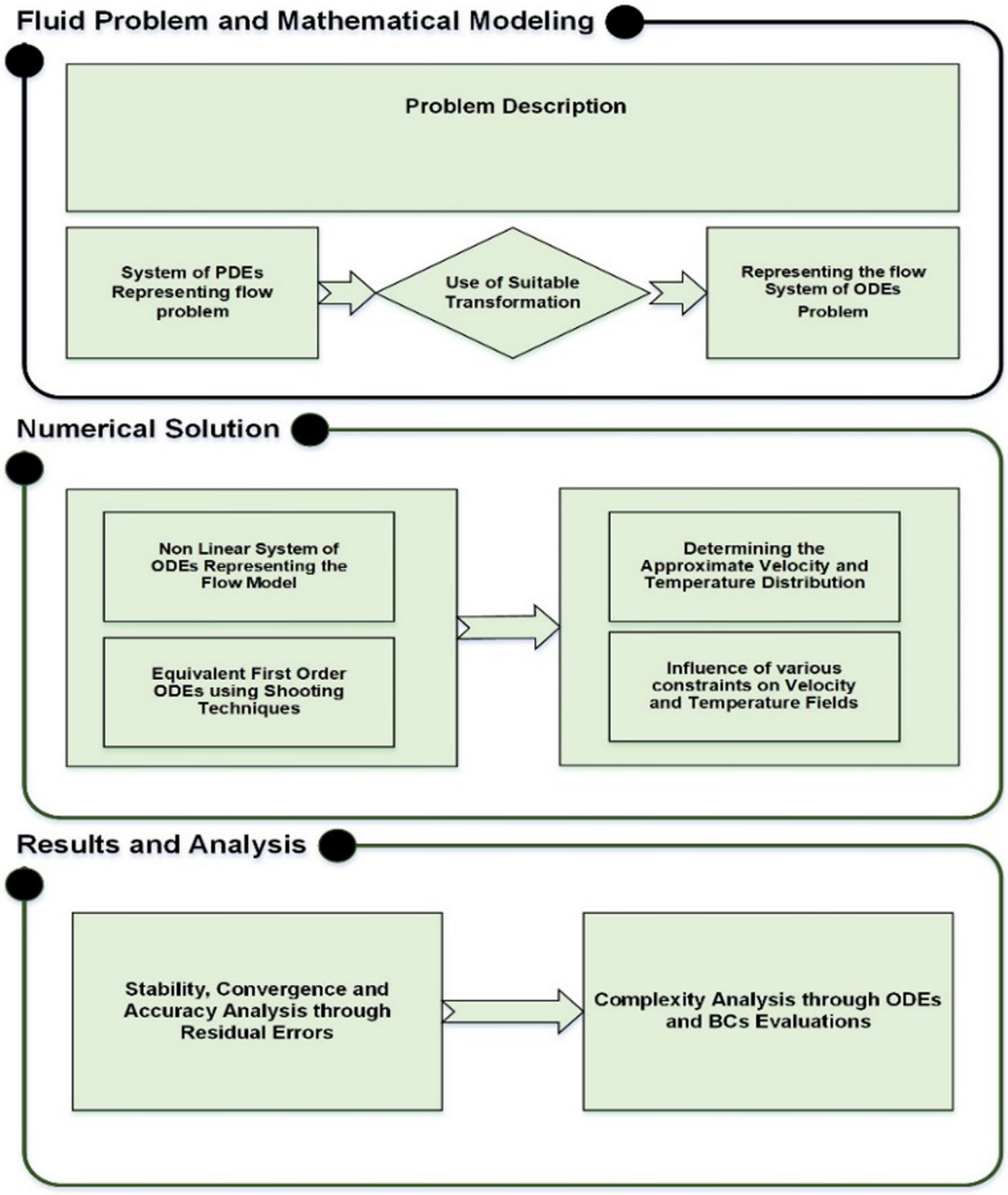

Figure 2: Description of the study.

with cross fluid over the stretching sheet is discussed by Shah *et al.* [9]. Mass transfer of nanoparticles of Carreau fluid with multiple features is revealed by Ayub *et al.* [10]. Activation role under magnetized flow, thermal radiation, buoyancy forces, *etc.*, is countered by several investigators [11–14].

Pumping or mixing fluids in microdevices can be accomplished using an electromagnetic body force (a Lorentz force) created by the interplay of an applied magneto force and an electrical currents that is typically provided outside. Magnetohydrodynamics (MHD) has long been the subject of considerable research due to its huge relevance in a variety of domains ranging from environmental phenomena such as geophysical and astrophysical to various technical applications such as plasma confinement, liquid metal, electromagnetic casting, and so on. Researchers in MHD natural convection completed a wide variety of research. To judge the

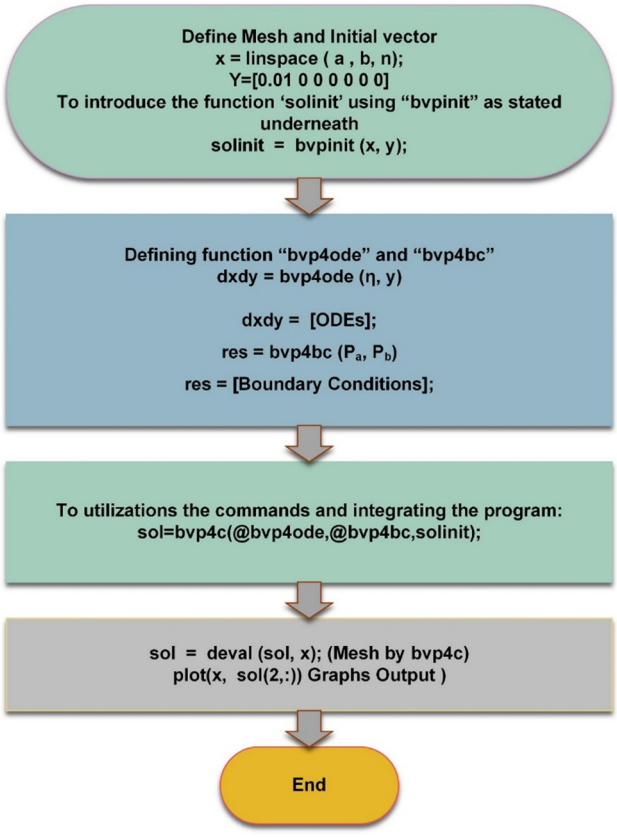

Figure 3: Description of bvp4c method.

key properties of fluid behavior under the influence of magnetic effect is called MHD flow. MHD keeps its vital application in many maladies that are dangerous to health, cancer tumor, and cure like healing wounds when bleeding is at its peak, and the most important key application is magneto resonance imaging which

Table 1: Verification table

β	Ali *et al.* [25]	Present study
0.0	0.469646	0.476461
0.3	0.476403	0.484032
0.6	0.997474	0.987435
1.2	1.335337	1.357343

presents an internal sketch of the brain [15–18]. The inclined magnetic effect of cross nanofluid with Brownian motion and the chemical process has been hashed out by Wahab *et al.* [19]. Khan *et al.* [20] investigated numerical solution of Carreau nanofluid keeping the orthogonal magnetic effect. The effect of perpendicular and inclined magnetic dipole combined with several effects like thermal radiation, heat sink source, and other numerous parameters are countered by different scholars [21–23] in detail.

The phenomenon of bringing the random particles into consideration and analysis of random motion is called Brownian motion. It achieves superb praise in the field of general science and the biological era of science. It is the result of continued collisions of molecules with the around medium. It has its influence in many areas of practical science like engineering and medicine [24–28]. The Brownian motion process of cross nanofluid with many features is discussed by Sabir *et al.* [29]. A micropolar fluid model with thermophoresis and Brownian motion under the influence of magnetic effect is revealed by ref. [30].

In this effort of investigation, our eye is on the melting process of energy under the influence of the inclined magnetic field of cross nanofluid over the geometry of wedge. The infinite shear rate viscosity model of

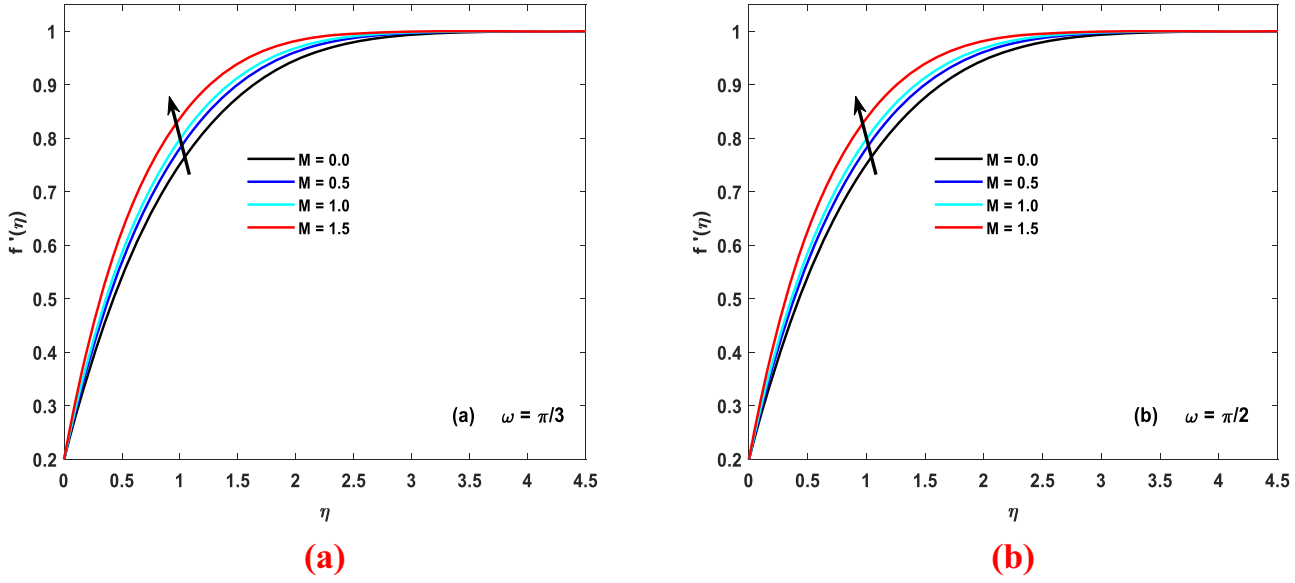

Figure 4: (a) and (b) Numerical consequences of *M* on the distribution of momentum of cross fluid.

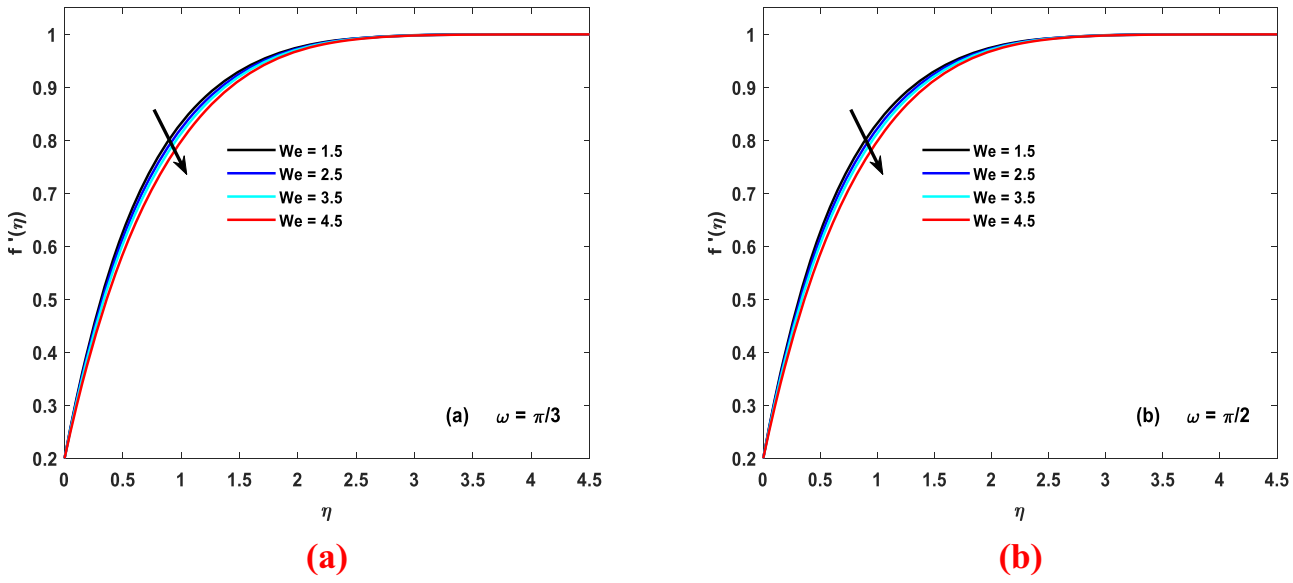

Figure 5: (a) and (b) Numerical consequences of We on the distribution of momentum of cross fluid.

the cross model is taken into consideration. A discussion of the mathematical formulation of the present article is presented in the next section.

2 Representation of mathematical formulation process

We assumed that there is a two-dimension (2D) fluid flowing over the Falkner-Skan wedge geometry. Characteristics of the assumed fluid flow are unsteadiness and incompressibility. There is assumed inclined magnetic field impact with infinite shear rate of viscosity model of cross fluid. The geometry look is seen in Figure 1.

When the wedge is stretching with velocity $U_e\left(=\frac{ax^m}{1-ct}\right)$ (with $ct < 1$), then the fluid velocity becomes free $U_w\left(=\frac{bx^m}{1-ct}\right)$ (with $ct < 1$) and it is called free stream velocity. a, b, and c involved in stretching and free stream velocity are positive constants and m is restricted by the interval [0,1]. Stretchiness and contraction of the

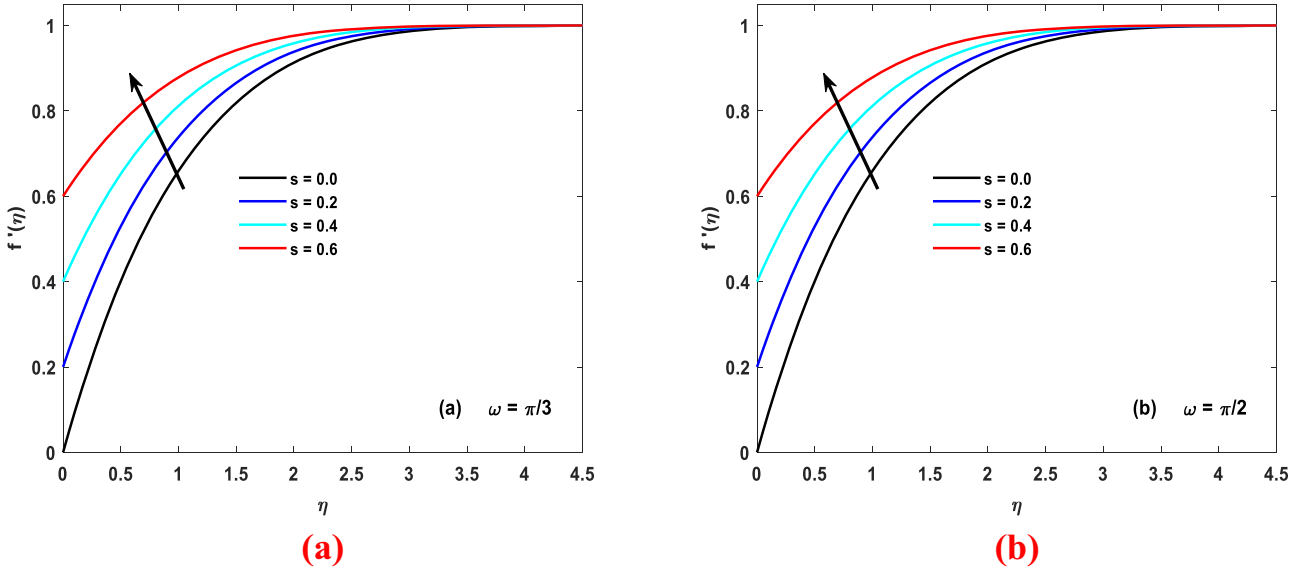

Figure 6: (a) and (b) Numerical consequences of s on the distribution of momentum of cross fluid.

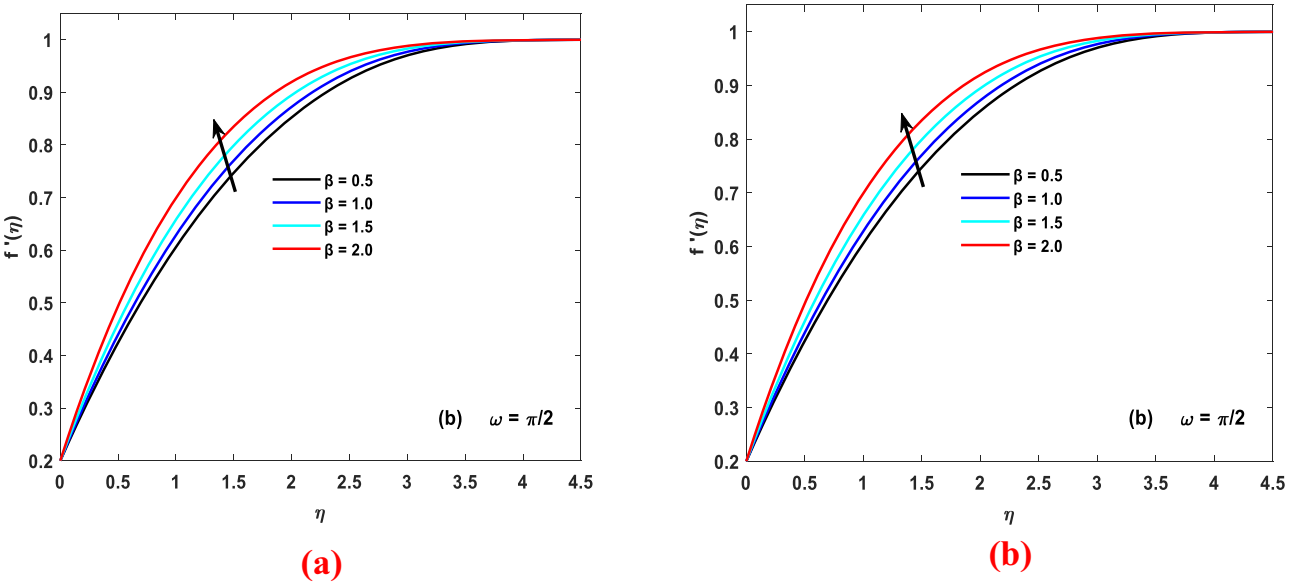

Figure 7: (a) and (b) Numerical consequences of β on the distribution of momentum of cross fluid.

wedge are shown by the mathematical relation of $U_w(x, t) > 0$ and $U_w(x, t) < 0$, respectively. $\Omega = \beta\pi$ is the wedge angle. The mathematics of assumed flow is described through the following equations and modeling.

$$\left.\begin{aligned} \text{Velocity visibity} &= [u(x, y, t), v(x, y, t)] = V, \\ \text{Tempreture visibity} &= T(x, y, t) = T, \\ \text{Concentration visibity} &= C(x, y, t) = C. \end{aligned}\right\} \quad (1)$$

3 Governing equations and infinite shear rate viscosity model of cross fluid

Viscosity model of cross fluid in terms of infinite shear rate [31] is given as

$$\mu(\dot{\gamma}) - \mu_\infty - \mu_0[1 + (\Gamma\dot{\gamma})^n]^{-1} + [1 + (\Gamma\dot{\gamma})^n]^{-1}\mu_\infty = 0, \quad (2)$$

$$\mu(\dot{\gamma}) - \mu_\infty\beta^* = [1 + (\Gamma\dot{\gamma})^n]^{-1} - \beta^*[1 + (\Gamma\dot{\gamma})^n]^{-1}. \quad (3)$$

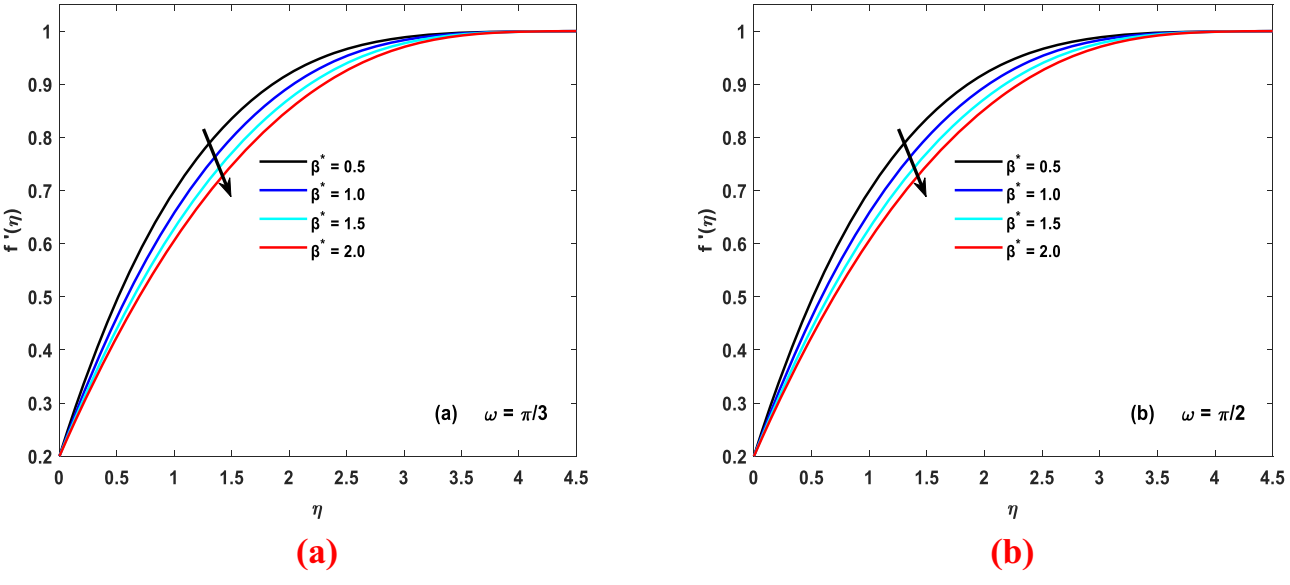

Figure 8: (a) and (b) Numerical consequences of β^* on the distribution of momentum of cross fluid.

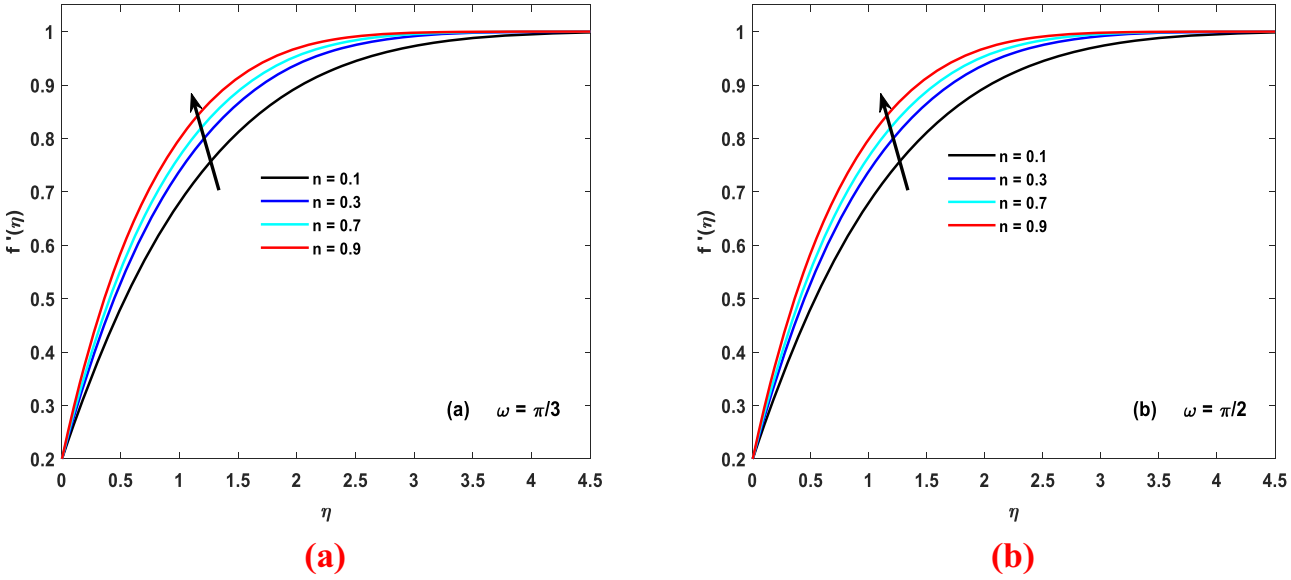

Figure 9: (a) and (b) Numerical consequences of n on the distribution of momentum of cross fluid.

Equations of motion, energy, and mass transport in the form of partial differential equations (PDEs) [32] are

$$\begin{aligned}&\frac{\partial u}{\partial t}+u\left(\frac{\partial u}{\partial x}\right)+v\left(\frac{\partial u}{\partial y}\right)=\frac{\partial U_e}{\partial t}+U_e\frac{\partial U_e}{\partial x}\\&+v\left(\beta^*\left(\frac{\partial^2 u}{\partial y^2}\right)+\left(\frac{\partial^2 u}{\partial y^2}\right)[1+(\Gamma\dot{\gamma})^n]^{-1}-\beta\right.\\&\left.^*\left(\frac{\partial^2 u}{\partial y^2}\right)[1+(\Gamma\dot{\gamma})^n]^{-1}\right)\\&-n\nu(1-\beta^*)\Gamma^n\left(\frac{\partial^2 u}{\partial y^2}\right)^n\left[\frac{1}{1+(\Gamma u_y)^n}\right]\left(\frac{\partial u}{\partial y}\right)^n\\&+\frac{\sigma^* B^2(t)}{\rho}\sin^2(\omega)(U_e-u),\end{aligned}\tag{4}$$

$$\begin{aligned}&[(\rho c)_f]\left[\frac{\partial T}{\partial t}+u\left(\frac{\partial T}{\partial x}\right)+v\left(\frac{\partial T}{\partial x}\right)\right]\\&=[(\rho c)_f]D_B\tau\left[\frac{1}{D_B\tau\alpha^{-1}}\left(\frac{\partial^2 T}{\partial y^2}\right)+\left(\frac{\partial T}{\partial y}\frac{\partial C}{\partial y}\right)\right.\\&\left.+\frac{1}{D_B\tau}\left[\frac{T_\infty}{D_T}\right]^{-1}\left(\frac{\partial C}{\partial y}\right)^2\right]+\frac{Q_0}{D_B\tau}(T-T_m),\end{aligned}\tag{5}$$

$$\begin{aligned}&u\left(\frac{\partial C}{\partial x}\right)+v\left(\frac{\partial C}{\partial y}\right)=D_B\left(\frac{\partial^2 C}{\partial y^2}\right)-\frac{\partial C}{\partial t}+\frac{D_T}{T_\infty}\left(\frac{\partial^2 T}{\partial y^2}\right),\\&-kc^2(C-C_\infty)\times(T_\infty{}^{-1}T)^m e^{\left(-\frac{Ea}{kT}\right)}\end{aligned}\tag{6}$$

$$U_e=\frac{ax^m}{1-ct},\beta^*=\frac{\mu_\infty}{\mu_0},\delta=\left[\frac{T_\infty}{T_m-T_\infty}\right]^{-1},$$

$$E=[K_\infty T_\infty]^{-1}Ea,\sigma=\left[\frac{a}{kc^2}\right]^{-1},$$

$$\left.\begin{aligned}&u=sU_e,v=0,T=T_m,C=C_m\quad\text{at}\quad y=0,\\&u\to U_e,\quad T\to T_\infty,C\to C_\infty\quad\text{as}\quad y\to\infty.\end{aligned}\right\}\tag{7}$$

With melting conditions [33]

$$\frac{k}{\rho}(T_y)\Big|_{y=0}=-\lambda-(T_m-T_0)c_s;T_y=\frac{\partial T}{\partial y}.\tag{8}$$

Using transformation

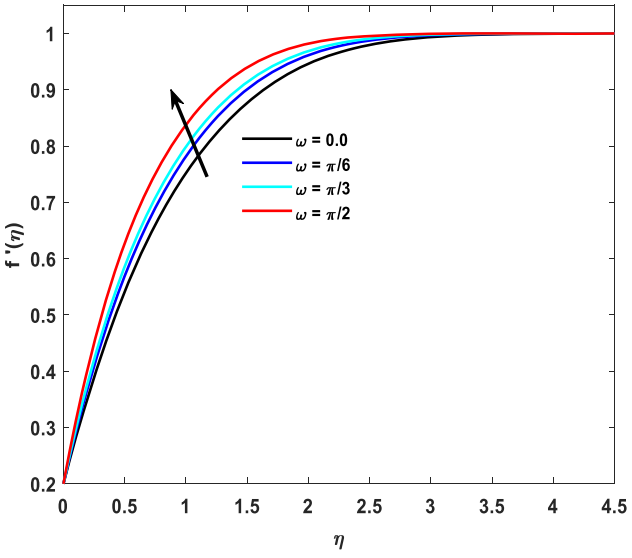

Figure 10: Numerical consequences of ω on the distribution of momentum of cross fluid.

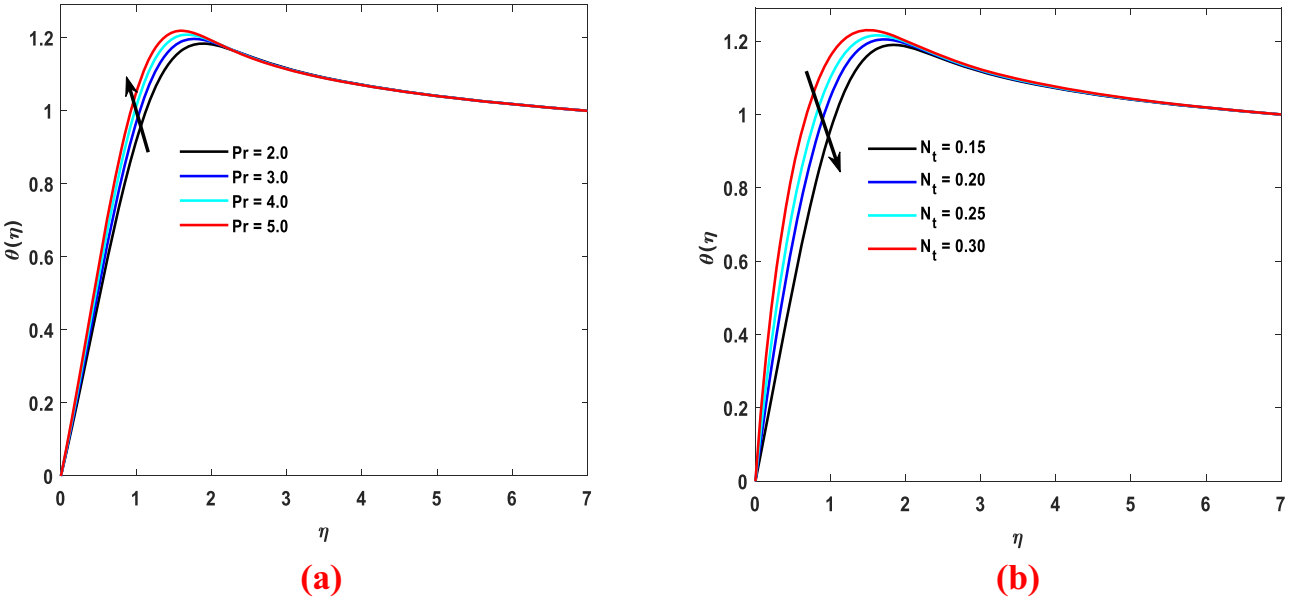

Figure 11: (a) and (b) Numerical consequences of the distribution of energy on varying the numerical values of Pr and Nt.

$$\left.\begin{aligned} &\zeta(x,y,t) = f(\eta)\sqrt{\frac{\lceil m+1\rceil^{-1}}{\lceil 2\nu x U_e\rceil^{-1}}},\\ &\theta(\eta)(T_\infty - T_m) = (T - T_m),\\ &\phi(\eta)\times(C_\infty - C_m) = (C - C_m),\\ &\text{with}\quad \eta\sqrt{2} = y\sqrt{\frac{U_e}{\nu\lceil m+1\rceil^{-1}x}}. \end{aligned}\right\} \tag{9}$$

Obtained ordinary differential equations (ODEs) from the system of PDEs by using Eq. (9) in Eqs. (4–6)

$$\begin{aligned} &\beta^*\lceil 1+\lceil \mathrm{We}f''\rceil^n\rceil^2 f''' - \left\{A\left(f' + \frac{1}{2}\eta f'' - 1\right)[1\right.\\ &\qquad \left. + (\mathrm{We}f'')^n] - ff''[1+(\mathrm{We}f'')^n]\right\}\\ &\qquad + \beta(f'^2 - 1)(1+(\mathrm{We}f'')^n)\\ &\qquad + (1-(n-1)(\mathrm{We}f'')^n)(1-\beta^*)f'''\\ &\qquad + M^2\sin^2(\omega)f' = 0, \end{aligned} \tag{10}$$

$$\theta'' - Q\theta = -\mathrm{Pr}[N_b\phi'\theta' + f\theta' - A\eta\theta' + N_t(\theta')^2], \tag{11}$$

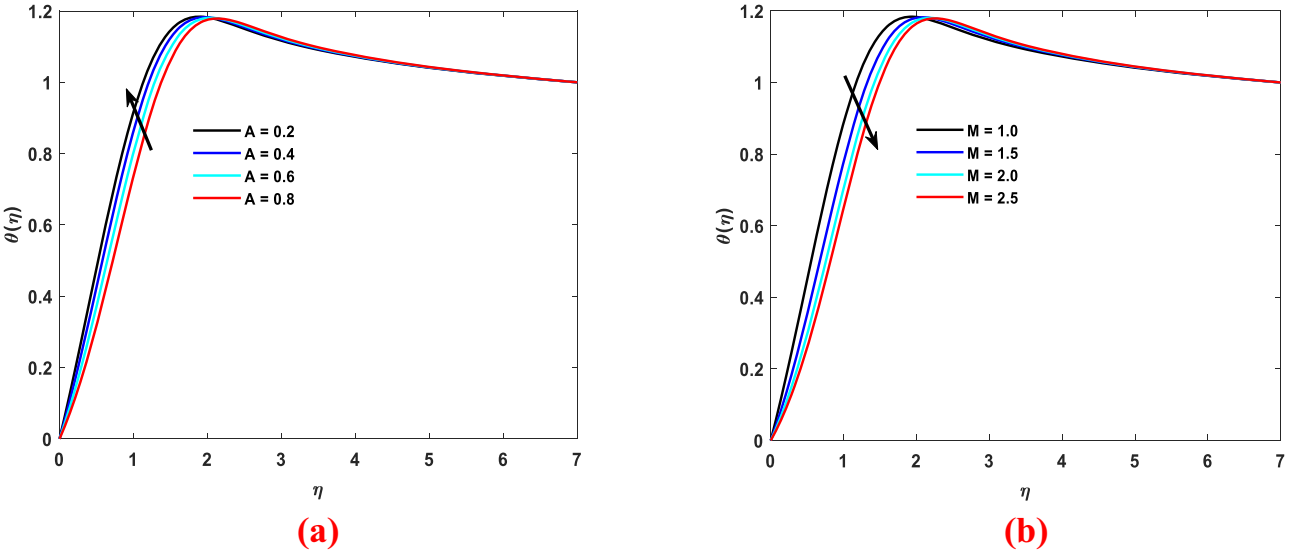

Figure 12: (a) and (b) Numerical consequences of the distribution of energy on varying the numerical values of *A* and *M*.

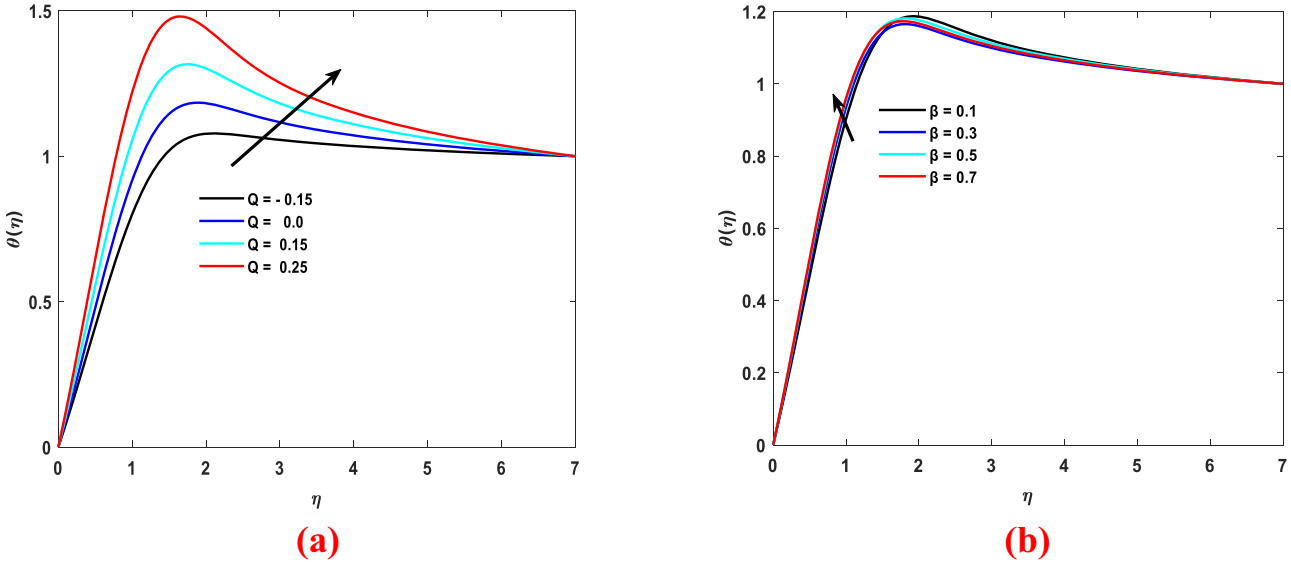

Figure 13: (a) and (b) Numerical consequences of the distribution of energy on varying the numerical values of Q and β.

$$\phi'' + \mathrm{Sc}\left[f \times \phi' - A\eta\phi' + \left(\frac{N_b}{N_t}\right)^{-1}\theta'' - \sigma(1+\delta\theta)^m \phi e^{\left(-\frac{E}{1+\delta\theta}\right)}\right] = 0, \tag{12}$$

subject to boundary conditions

$$\left.\begin{aligned} N_b\phi' - N_t\theta' = 0, f' = s, \theta = 0, M\theta + \mathrm{Pr}f = 0, \text{ at} \\ \eta = 0, \\ f' \to 1, \theta \to 1, \phi \to 1 \quad \text{as} \quad \eta \to \infty, \end{aligned}\right\} \tag{13}$$

Where

$$2\nu\mathrm{We}^2 = \frac{b^3(m+1)}{\nu^{-1}(x)^{-3m+1}}, \quad \mathrm{Pr} = \frac{\mu c_p}{k}, N_t = \frac{\tau D_T(T_m - T_\infty)}{\nu T_\infty},$$
$$N_b = \frac{\nu^{-1}}{[\tau D_B(C_w - C_\infty)]^{-1}}, \quad M = [\lambda + (c_s T_m - c_s T_0)]^{-1}[c_p(T_\infty - T_m)],$$
$$\beta = \frac{2m}{m+1}, \quad B^* = \frac{\mu_\infty}{\mu_0}, A = \frac{c}{(m+1)ax^{m-1}}, Q = \frac{2Q_0(1-ct)}{\rho c_p(m+1)ax^{m-1}}, \quad \mathrm{Sc} = \frac{\nu}{D_B}.$$

Mathematics of drag real-life quantities (force and rate of heat transfer)

$$\frac{\rho U_e^2 C_{fx}}{\tau_w|_{y=o}} = 1, \tag{14}$$

where C_{fx} is the dimensionless aspect defined as

$$\frac{\sqrt{2}\,\mathrm{Re}_2^{\frac{1}{2}} C_{fx}}{f''(0)\sqrt{(m+1)}[\beta^* + (1-\beta^*)]} = [1 + (\mathrm{We}f''(0))^n]^{-1},$$

and

$$\frac{\mathrm{Nu}_x(T_\infty - T_m)}{x} = \left(\frac{\partial T}{\partial y}\right)|_{y=0}. \tag{15}$$

The dimensionless version of Nu_x is

$$\mathrm{Re}_x^{-\frac{1}{2}}\mathrm{Nu}_x\sqrt{\left(\frac{m+1}{2}\right)^{-1}} = -\theta'(0), \tag{16}$$

where $\mathrm{Re} = \frac{xU_e}{\nu}$ is mathematical expression of local Reynolds number. Figure 2 defines the fluid problem and mathematical modeling of the current problem.

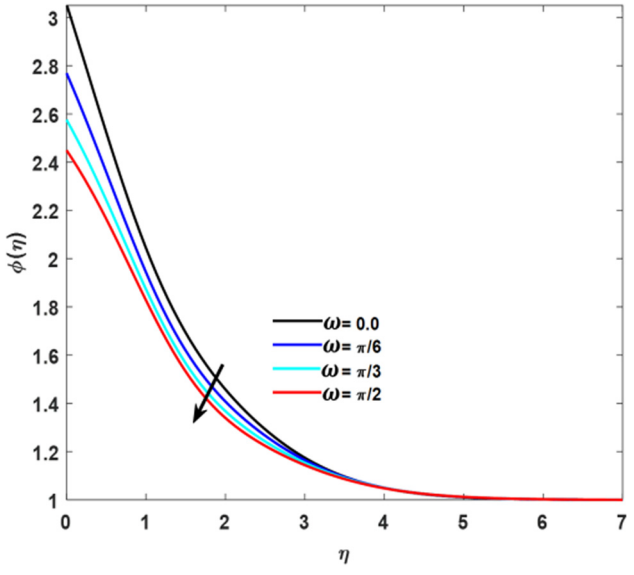

Figure 14: Numerical consequences of the distribution of energy on varying the numerical values of ω.

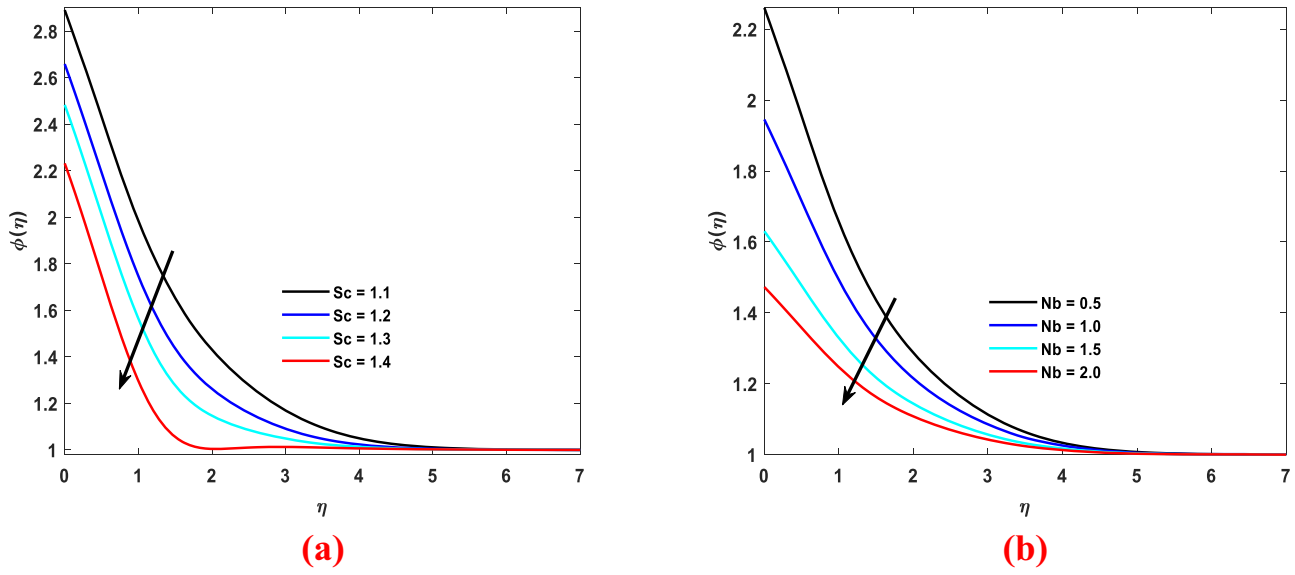

Figure 15: (a) and (b) Numerical consequences of concentration profile *via* Sc and Nb.

4 Solution methodology

In this section, process of the numerical solution is presented. Bvp4c method [34–41] is applied to move the boundary value problem into the initial value problem. The complete procedure is given in Figure 3.

5 Validation of work

Table 1 shows the smooth agreement with old literature.

6 Results and discussion

This Section presents the detailed consequences of several physical parameters on the distribution of velocity, temperature, and transport of mass.

6.1 Velocity profile $f'(\eta)$

All major facts based on results concerning velocity are shown in Figures 4–10. Reports of M and We on velocity are shown in Figures 4(a) and (b) and 5(a) and (b). Behavior of

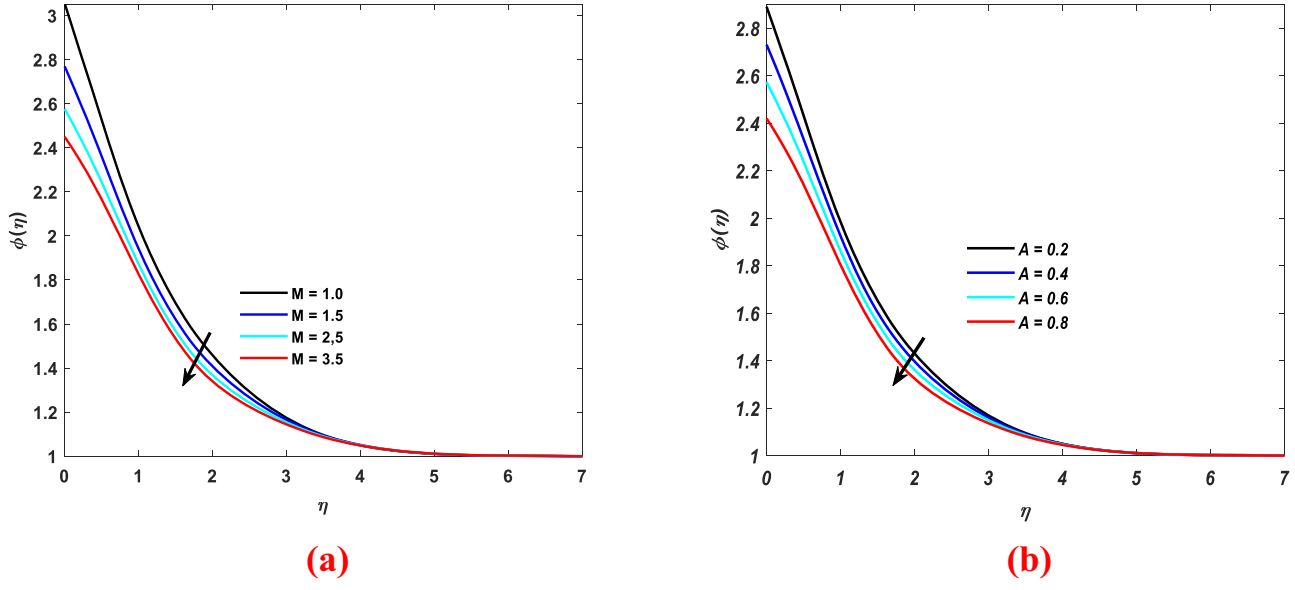

Figure 16: (a) and (b) Numerical consequences distribution of mass transport on varying the numerical values of M and A.

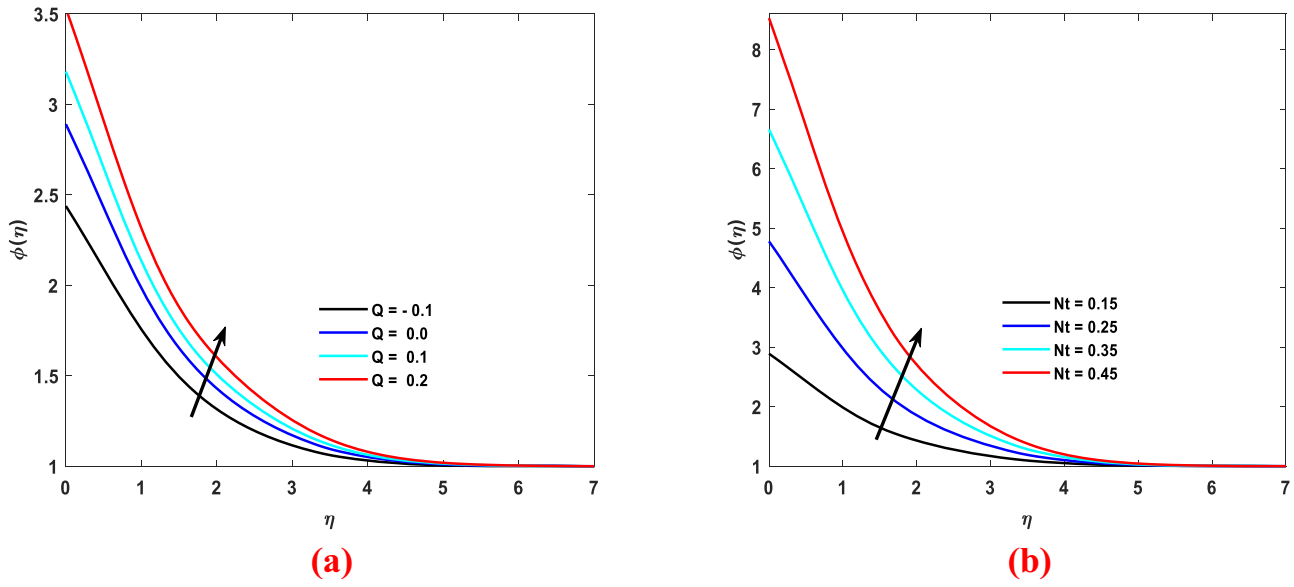

Figure 17: (a) and (b) Numerical consequences of the distribution of mass transport on varying the numerical values of Q and Nt.

nanoparticles seems depressed for the increase in We but boosts for ascending values of M. We shows relaxation time and M causes Lorentz force due to these factors, the velocity varies for M and We. An inclined angle is caused to create more Lorentz force, as the inclined angle is going orthogonal, due to the Lorentz force effect, velocity decreased. The influence of velocity ratios on the velocity is displayed in Figure 6(a) and (b). The symbol s is the velocity ratio, so greater numerical values of this parameter enhance the fluid viscosity which provides a decrement in the fluid motion, and velocity decreases. Figures 7(a) and (b) and 8(a) and (b) disclose the influence of β and β^*, respectively. On increasing the values of β and β^*, velocity seems to be depressed due to the flow moving across the wedge. It is well established that the fluid velocity escalates due to an enhancement in wedge angle which amplifies velocity. The velocity of the fluid diminishes owing to magnification in β^*. It is noticed from Figure 9(a) and (b) that the velocity of fluid increases by improving the power law index n. The fluid behavior is

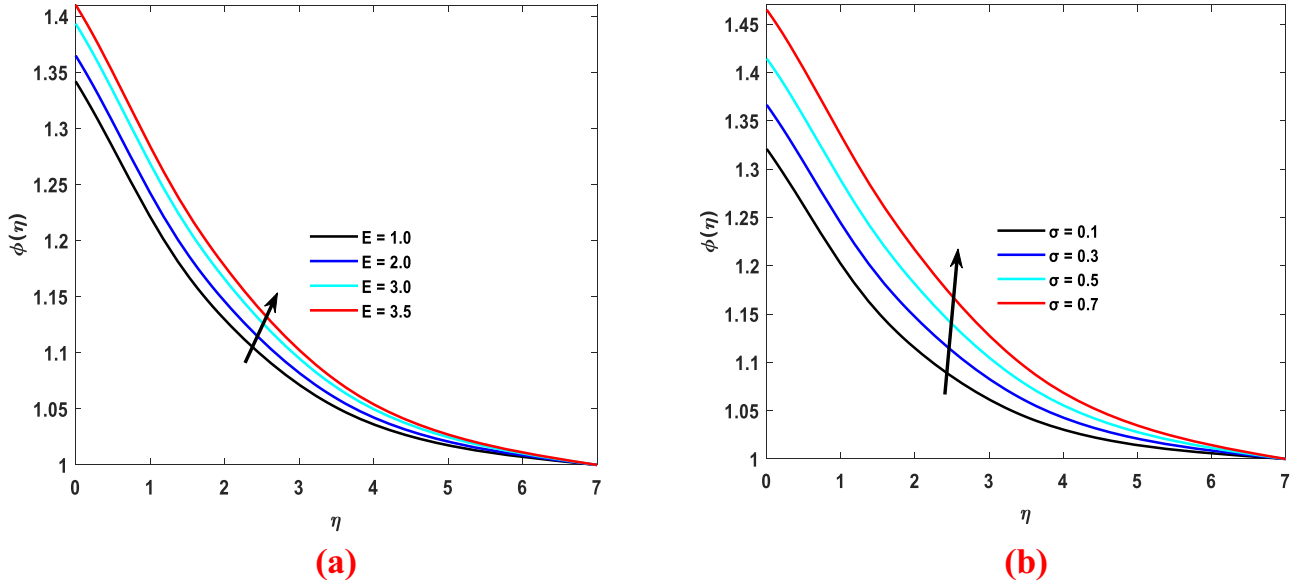

Figure 18: (a) and (b) Numerical consequences of distribution of mass transport on varying the numerical values of E and σ.

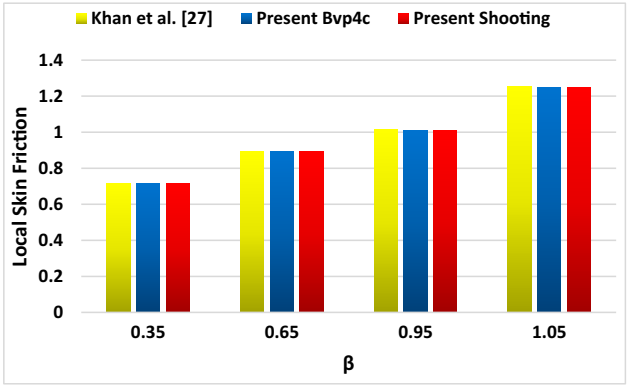

Figure 19: Numerical consequences of local skin friction coefficient with β.

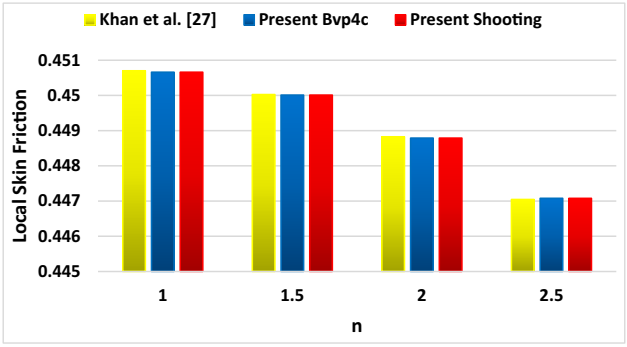

Figure 21: Numerical consequences of local skin friction coefficient with n.

shear thinning by the virtue of a magnification in n which diminishes the viscosity phenomenon and increases the velocity. From Figure 10 it is observed that the velocity of the fluid augments owing to magnification in wedge angle.

6.2 Temperature profile $\theta(\eta)$

The results of scrutiny of $\theta(\eta)$ distribution with the attached parameter are shown in Figures (11)–(14). Figure 11(a) and (b) reveals the effect of Prandtl and thermophoresis parameters. With the increase in Pr, the temperature profile increases, and it decreases due to a decrement in thermal conductivity of thermophoresis. Thermal diffusivity amplifies by the virtue of an amplification in Pr which amplifies the heat transfer rate and the temperature field. The molecules diffuse from the hotter surface toward the colder surface on behalf of an incremental change in the thermophoresis parameter which diminishes the temperature inside the fluid.

Figure 12(a) and (b) launches the resultant effect of the unsteadiness parameter and melting parameter. The unsteadiness parameter boosts the temperature but the melting effect causes to lower the temperature field. It is well established that the viscosity of the fluid increases owing to an amplification in the unsteadiness parameter which amplifies the fluid viscosity. Viscosity is inversely related to temperature. That is why a positive change in the unsteadiness parameter depreciates fluid viscosity and escalates the temperature field. It is noted that a positive variation in melting parameter M diminishes the temperature field. The heat generation/absorption parameter has a direct relation with temperature and due to the generation of heat, temperature increases and the same result is achieved for wedge angle.

This fact is shown in Figure 13(a). More heat enters inside the fluid as a result of magnification in the heat generation parameter which amplifies the heat inside the fluid and temperature field as well. The passage of the fluid flow diminishes owing to an increment in wedge angle and molecules collide more randomly which

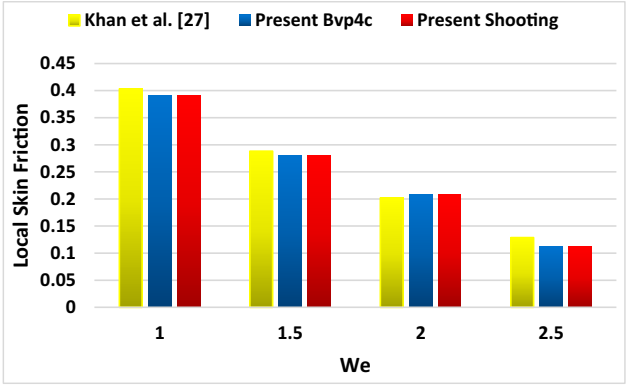

Figure 20: Numerical consequences of local skin friction coefficient with We.

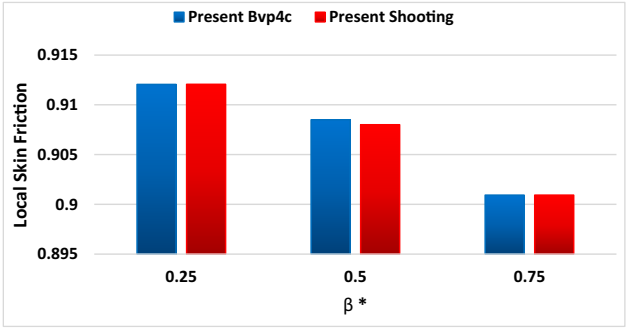

Figure 22: Numerical consequences of local skin friction coefficient with β^*.

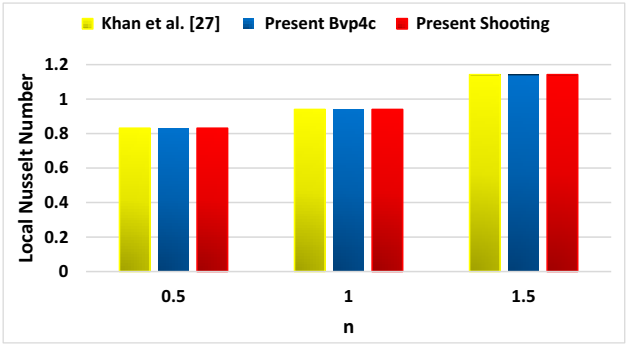

Figure 23: Numerical consequences of local Nusselt coefficient with n.

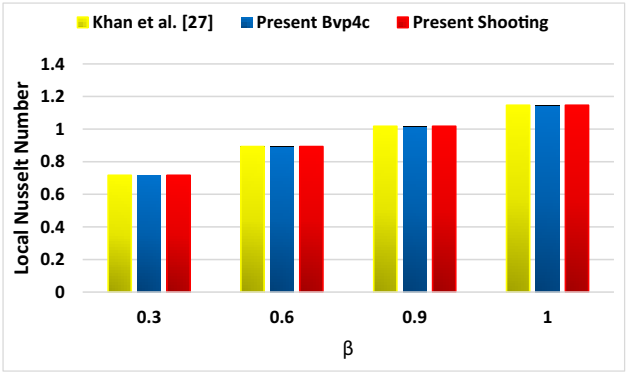

Figure 25: Numerical consequences of local skin Nusselt coefficient with β.

enhances the thermal conductivity of the fluid and temperature field as well, as shown in Figure 13(b). It is noticed from Figure 14 that the temperature, as well as heat transfer rate, diminishes when there is a positive change in an inclined angle.

6.3 Concentration of nanoparticle $\phi(\eta)$

The results of scrutiny of $\phi(\eta)$ distribution with the attached parameter are shown in Figures 15–18. Figure 15(a and b) reveals the effect of Schmidt number Sc and Brownian parameter Nb, as a result the profile of $\phi(\eta)$ is seen depressed for both the mentioned parameters. Due to mass diffusivity and increment in the collusion between molecules, Schmidt diffusivity is inversely related to mass diffusivity. A positive variation in mass diffusivity diminishes the concentration profile which diminishes the concentration field. Molecules collide more randomly as a result of magnification in Nb which amplifies temperature and molecules from a region of lower concentration to the higher which creates abatement in the concentration field. The melting process reduces the concentration and as a result temperature declines and also, the unsteadiness parameter is decreasing the temperature. Effects of M and A are shown in Figure 16(a) and (b). From Figure 17(a) and (b), it can be seen that the concentration profile *via* Q and Nt is increasing due to heat generation effect. It is noticed that the heat transfer rate amplifies due to the change in Q which amplifies the mass diffusion phenomenon and concentration of the fluid as well. The molecules diffuse from a region of lower concentration to a higher one as a result of a magnification in Nt which brings about an amplification in the concentration field. Activation energy and σ effect on mass transfer field is presented in Figure 18(a) and (b). Increment in E increases the concentration because activation energy provides the energy to activate the chemical reaction. The concentration profile enlarges as a result of a magnification in E which provides substantial energy to process the reaction and strengthen the concentration field. Amplification in reaction rate parameter σ amplifies the overall activation energy phenomenon and concentration of the fluid.

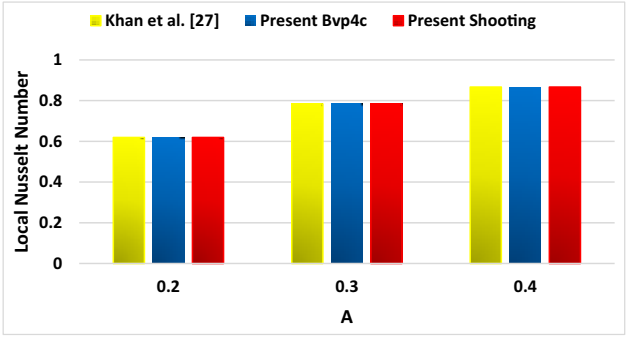

Figure 24: Numerical consequences of local Nusselt coefficient with A.

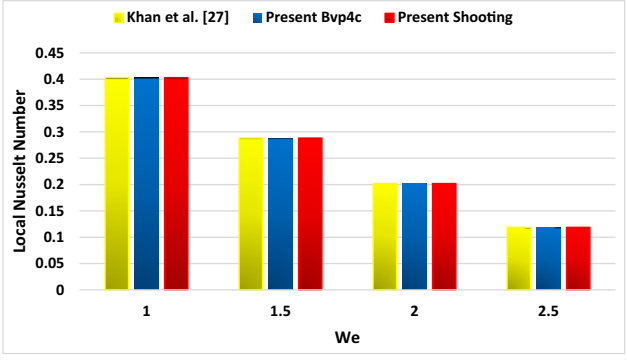

Figure 26: Numerical consequences of local skin Nusselt coefficient with We.

6.4 Local skin friction and Nusselt number

In this section, the numerical aspect of physical quantities is presented *via* statistical graphs. Statistical Figures 19–22 are presented with attached numerical physical parameters. Figures 19–22 represent the comparison analysis of the obtained results with those obtained by Ali *et al.* [25], bvp4c, and shooting for the case of surface drag coefficient due to variation in various dimensionless parameters like β, We, n, and β^*. From the figures, it is noticed that the incremental change in surface drag is observed in the case of β but decremented change is noticed in the case of the remaining parameters.

From Figures 23–26, it is observed that the obtained results are quite reliable in comparison to that in the already available literature, bvp4c, and shooting technique. The change in heat rate escalates owing to magnification in n, A, and β but diminishes in the case of an increment in We.

7 Conclusion

The primary goal of this research is to acquire the numerical and tabular results of infinite shearing rate viscid of a cross rheological model including Brownian diffusion, thermophoretic, activation energy, and heat production under melting heat conditions. The gist of the current study is presented with sum-up points.

1) Activation energy promotes mass transport.
2) Due to imposed inclined magnetic field, Lorentz force is generated, hence the velocity of cross nanofluid is decreased.
3) Inclined magnetic effect causes decrease in the velocity of cross nanofluid.
4) For greater infinite shear rate viscosity parameter β^*, magnitude of velocity profile decreases.
5) Concentration profile *via* Q and Nt increases due to the heat generation effect.
6) Increment in E increases concentration because activation energy provides the energy to activate the chemical reaction.

The bvp4c technique could be applied to a variety of physical and technical challenges in the future [42–52]. Some recent developments exploring the significance of the considered research domain are reported in the studies [53–68].

Acknowledgments: The authors would like to thank the Deanship of Scientific Research at Umm Al-Qura University for supporting this work by Grant Code: (23UQU4331317DSR108).

Funding information: The Deanship of Scientific Research at Umm Al-Qura University with Grant Code: (23UQU4331317DSR108).

Author contributions: All authors have accepted responsibility for the entire content of this manuscript and approved its submission.

Conflict of interest: The authors state no conflict of interest.

References

[1] Mani D, Saranprabhu MK, Rajan KS. Intensification of thermal energy storage using copper-pentaerythritol nanocomposites for renewable energy utilization. Renew Energy. 2021;163:625–34.
[2] Wang X, Lu C, Rao W. Liquid metal-based thermal interface materials with a high thermal conductivity for electronic cooling and bioheat-transfer applications. Appl Therm Eng. 2021;192:116937.
[3] Ezenwa IC, Yoshino T. Martian core heat flux: Electrical resistivity and thermal conductivity of liquid Fe at Martian core PT conditions. Icarus. 2021;360:114367.
[4] Ayub A, Wahab HA, Hussain Shah SZ, Shah SL, Sabir Z, Bhatti S. On heated surface transport of heat bearing thermal radiation and MHD Cross flow with effects of nonuniform heat sink/source and buoyancy opposing/assisting flow. Heat Transf. 2021;50(6):6110–28.
[5] Asjad MI, Ali R, Iqbal A, Muhammad T, Chu YM. Application of water based drilling clay-nanoparticles in heat transfer of fractional Maxwell fluid over an infinite flat surface. Sci Rep. 2021;11(1):1–14.
[6] Waqas H, Kafait A, Alghamdi M, Muhammad T, Alshomrani AS. Thermo-bioconvectional transport of magneto-Casson nanofluid over a wedge containing motile microorganisms and variable thermal conductivity. Alex Eng J. 2021;61(3):2444–54.
[7] Ayub A, Sabir Z, Altamirano GC, Sadat R, Ali MR. Characteristics of melting heat transport of blood with time-dependent cross-nanofluid model using Keller–Box and bvp4c method. Eng Computers. 2021;38:1–15. doi: 10.1007/s00366-021-01406-7.
[8] Ayub A, Wahab HA, Shah SZ, Shah SL, Darvesh A, Haider A, et al. Interpretation of infinite shear rate viscosity and a non-uniform heat sink/source on a 3D radiative cross nanofluid with buoyancy assisting/opposing flow. Heat Transf. 2021;50(5):4192–232.

[9] Shah SZ, Wahab HA, Ayub A, Sabir Z, haider A, Shah SL. Higher order chemical process with heat transport of magnetized cross nanofluid over wedge geometry. Heat Transf. 2021;50(4):3196–219.
[10] Ayub A, Sabir Z, Le DN, Aly AA. Nanoscale heat and mass transport of magnetized 3-D chemically radiative hybrid nanofluid with orthogonal/inclined magnetic field along rotating sheet. Case Stud Therm Eng. 2021;26:101193.
[11] Prakash J, Siva EP, Tripathi D, Kuharat S, Bég OA. Peristaltic pumping of magnetic nanofluids with thermal radiation and temperature-dependent viscosity effects: modelling a solar magneto-biomimetic nanopump. Renew Energy. 2019;133:1308–26.
[12] Hamid M, Usman M, Haq RU. Wavelet investigation of Soret and Dufour effects on stagnation point fluid flow in two dimensions with variable thermal conductivity and diffusivity. Phys Scr. 2019;94(11):115219.
[13] Prakash J, Sharma A, Tripathi D. Thermal radiation effects on electroosmosis modulated peristaltic transport of ionic nanoliquids in biomicrofluidics channel. J Mol Liq. 2018;249:843–55.
[14] Siddiqui MA, Riaz A, Khan I, Nisar KS. Augmentation of mixed convection heat transfer in a lid-assisted square enclosure utilizing micropolar fluid under magnetic environment: A numerical approach. Results Phys. 2020;18:103245.
[15] Ali A, Saleem S, Mumraiz S, Saleem A, Awais M, Marwat DK. Investigation on TiO_2–Cu/H_2O hybrid nanofluid with slip conditions in MHD peristaltic flow of Jeffrey material. J Therm Anal Calorim. 2021;143(3):1985–96.
[16] Tian MW, Rostami S, Aghakhani S, Goldanlou AS, Qi C. A techno-economic investigation of 2D and 3D configurations of fins and their effects on heat sink efficiency of MHD hybrid nanofluid with slip and non-slip flow. Int J Mech Sci. 2021;189:105975.
[17] Zhang XH, Abidi A, Ahmed AES, Khan MR, El-Shorbagy MA, Shutaywi M, et al. MHD stagnation point flow of nanofluid over a curved stretching/shrinking surface subject to the influence of Joule heating and convective condition. Case Stud Therm Eng. 2021;26:101184.
[18] Li YX, Alshbool MH, LV YP, Khan I, Khan MR, Issakhov A. Heat and mass transfer in MHD Williamson nanofluid flow over an exponentially porous stretching surface. Case Stud Therm Eng. 2021;26:100975.
[19] Wahab HA, Hussain Shah SZ, Ayub A, Sabir Z, Bilal M, Altamirano GC. Multiple characteristics of three-dimensional radiative Cross fluid with velocity slip and inclined magnetic field over a stretching sheet. Heat Transf. 2021;50(4):3325–41.
[20] Khan M, Irfan M, Ahmad L, Khan WA. Simultaneous investigation of MHD and convective phenomena on time-dependent flow of Carreau nanofluid with variable properties: dual solutions. Phys Lett A. 2018;382(34):2334–42.
[21] Khan NS, Gul T, Kumam P, Shah Z, Islam S, Khan W, et al. Influence of inclined magnetic field on Carreau nanoliquid thin film flow and heat transfer with graphene nanoparticles. Energies. 2019;12(8):1459.
[22] Mahanthesh B. Magnetohydrodynamic flow of Carreau liquid over a stretchable sheet with a variable thickness: the biomedical applications. Multidiscipline Modeling Mater Struct. 2020;16(5):1277–93.
[23] Animasaun IL, Koriko OK, Adegbie KS, Babatunde HA, Ibraheem RO, Sandeep N, et al. Comparative analysis between 36 nm and 47 nm alumina–water nanofluid flows in the presence of Hall effect. J Therm Anal Calorim. 2019;135(2):873–86.
[24] Irfan M. Study of Brownian motion and thermophoretic diffusion on non-linear mixed convection flow of Carreau nanofluid subject to variable properties. Surf Interfaces. 2021;23:100926.
[25] Ali M, Shahzad M, Sultan F, Khan WA, Shah SZH. Characteristic of heat transfer in flow of Cross nanofluid during melting process. Appl Nanosci. 2020;10(12):5201–10.
[26] Shah Z, Dawar A, Islam S. Influence of Brownian motion and thermophoresis parameters on silver-based Di-hydrogen CNTs between two stretchable rotating disks. Phys Scr. 2021;96(5):055205.
[27] Saghir MZ, Rahman MM. Brownian motion and thermophoretic effects of flow in channels using nanofluid: A two-phase model. Int J Thermofluids. 2021;10:100085.
[28] Zhang X, Xu Y, Zhang J, Rahmani A, Sajadi SM, Zarringhalam M, et al. Numerical study of mixed convection of nanofluid inside an inlet/outlet inclined cavity under the effect of Brownian motion using Lattice Boltzmann Method (LBM). Int Commun Heat Mass Transf. 2021;126:105428.
[29] Sabir Z, Ayub A, Guirao JL, Bhatti S, Shah SZH. The effects of activation energy and thermophoretic diffusion of nanoparticles on steady micropolar fluid along with Brownian motion. Adv Mater Sci Eng. 2020;2020:2010568.
[30] Ayub A, Wahab HA, Sabir Z, Arbi A. A note on heat transport with aspect of magnetic dipole and higher order chemical process for steady micropolar fluid. Computational Overview of Fluid Structure Interaction Book. London, UK: IntechOpen; 2020.
[31] Ayub A, Sabir Z, Shah SZH, Mahmoud SR, Algarni A, Sadat R, et al. Aspects of infinite shear rate viscosity and heat transport of magnetized Carreau nanofluid. Eur Phys J Plus. 2022;137(2):1–17.
[32] Shah SZH, Ayub A, Sabir Z, Adel W, Shah NA, Yook SJ. Insight into the dynamics of time-dependent cross nanofluid on a melting surface subject to cubic autocatalysis. Case Stud Therm Eng. 2021;27:101227.
[33] Wang F, Sajid T, Ayub A, Sabir Z, Bhatti S, Shah NA, et al. Melting and entropy generation of infinite shear rate viscosity Carreau model over Riga plate with erratic thickness: a numerical Keller Box approach. Waves Random Complex Media. 2022;1–25. doi: 10.1080/17455030.2022.2063991.
[34] Ayub A, Sabir Z, Shah SZH, Wahab HA, Sadat R, Ali MR. Effects of homogeneous-heterogeneous and Lorentz forces on 3-D radiative magnetized cross nanofluid using two rotating disks. Int Commun Heat Mass Transf. 2022;130:105778.
[35] Shah SZH, Fathurrochman I, Ayub A, Altamirano GC, Rizwan A, Núñez RAS, et al. Inclined magnetized and energy transportation aspect of infinite shear rate viscosity model of Carreau nanofluid with multiple features over wedge geometry. Heat Transf. 2022;51(2):1622–48.
[36] Ayub A, Wahab HA, Balubaid M, Mahmoud SR, Ali MR, Sadat R. Analysis of the nanoscale heat transport and Lorentz force based on the time-dependent Cross nanofluid. Eng Computers. 2022;1–20. doi: 10.1007/s00366-021-01579-1.
[37] Ayub A, Shah SZH, Sabir Z, Rao NS, Sadat R, Ali MR. Spectral relaxation approach and velocity slip stagnation point flow of

inclined magnetized cross-nanofluid with a quadratic multiple regression model. Waves Random Complex Media. 2022;1–25. doi: 10.1080/17455030.2022.2049923.
[38] Shah SL, Ayub A, Dehraj S, Wahab HA, Sagayam KM, Ali MR, et al. Magnetic dipole aspect of binary chemical reactive Cross nanofluid and heat transport over composite cylindrical panels. Waves Random Complex Media. 2022;1–24. doi: 10.1080/17455030.2021.2020373.
[39] Haider A, Ayub A, Madassar N, Ali RK, Sabir Z, Shah SZ, et al. Energy transference in time-dependent Cattaneo–Christov double diffusion of second-grade fluid with variable thermal conductivity. Heat Transf. 2021;50(8):8224–42.
[40] Sabir Z, Raja MAZ, Wahab HA, Altamirano GC, Zhang YD, Le DN. Integrated intelligence of neuro-evolution with sequential quadratic programming for second-order Lane–Emden pantograph models. Math Comput Simul. 2021;188:87–101.
[41] Darvesh A, Altamirano GC. Inclined magnetic dipole and nanoscale energy exchange with infinite shear rate viscosity of 3D radiative cross nanofluid. Heat Transf. 2022;51(4):3166–86.
[42] Jamshed W, Aziz A. Entropy analysis of TiO_2-Cu/EG casson hybrid nanofluid *via* CattaneoCchristov heat flux model. Appl Nanosci. 2018;8:1–14.
[43] Jamshed W, Nisar KS. Computational single phase comparative study of Williamson nanofluid in parabolic trough solar collector *via* Keller box method. Int J Energy Res. 2021;45(7):10696–718.
[44] Jamshed W, Devi SU, Nisar KS. Single phase-based study of Ag-Cu/EO Williamson hybrid nanofluid flow over a stretching surface with shape factor. Phys Scr. 2021;96:065202.
[45] Jamshed W, Nisar KS, Ibrahim RW, Shahzad F, Eid MR. Thermal expansion optimization in solar aircraft using tangent hyperbolic hybrid nanofluid: a solar thermal application. J Mater Res Technol. 2021;14:985–1006.
[46] Jamshed W, Nisar KS, Ibrahim RW, Mukhtar T, Vijayakumar V, Ahmad F. Computational frame work of Cattaneo-Christov heat flux effects on Engine Oil based Williamson hybrid nanofluids: A thermal case study. Case Stud Therm Eng. 2021;26:101179.
[47] Jamshed W, Mishra SR, Pattnaik PK, Nisar KS, Devi SSU, Prakash M, et al. Features of entropy optimization on viscous second grade nanofluid streamed with thermal radiation: A Tiwari and Das model. Case Stud Therm Eng. 2021;27:101291.
[48] Jamshed W, Nasir NA, Isa SS, Safdar R, Shahzad F, Nisar KS, et al. Thermal growth in solar water pump using Prandtl–Eyring hybrid nanofluid: a solar energy application. Sci Rep. 2021;11:18704.
[49] Jamshed W, Shahzad F, Safdar R, Sajid T, Eid MR, Nisar KS. Implementing renewable solar energy in presence of Maxwell nanofluid in parabolic trough solar collector: a computational study. Waves Random Complex Media. 2021;1–32. doi: 10.1080/17455030.2021.1989518.
[50] Jamshed W. Finite element method in thermal characterization and streamline flow analysis of electromagnetic silver-magnesium oxide nanofluid inside grooved enclosure. Int Commun Heat Mass Transf. 2021;130:105795.
[51] Jamshed W, Sirin C, Selimefendigil F, Shamshuddin MD, Altowairqi Y, Eid MR. Thermal characterization of coolant Maxwell type nanofluid flowing in parabolic trough solar collector (PTSC) used inside solar powered ship application. Coatings. 2021;11(12):1552.
[52] Jamshed W, Mohd Nasir NAA, Qureshi MA, Shahzad F, Banerjee R, Eid MR, et al. Dynamical irreversible processes analysis of Poiseuille magneto-hybrid nanofluid flow in microchannel: A novel case study. Waves Random Complex Media. 2022. doi: 10.1080/17455030.2021.1985185.
[53] Hussain SM, Goud BS, Madheshwaran P, Jamshed W, Pasha AA, Safdar R, et al. Effectiveness of nonuniform heat generation (Sink) and thermal characterization of a Carreau fluid flowing across a nonlinear elongating cylinder: A numerical study. ACS Omega. 2022;7(29):25309–20.
[54] Pasha AA, Islam N, Jamshed W, Alam MI, Jameel AGA, Juhany KA, et al. Statistical analysis of viscous hybridized nanofluid flowing *via* Galerkin finite element technique. Int Commun Heat Mass Transf. 2022;137:106244.
[55] Hussain SM, Jamshed W, Pasha AA, Adil M, Akram M. Galerkin finite element solution for electromagnetic radiative impact on viscid Williamson two-phase nanofluid flow *via* extendable surface. Int Commun Heat Mass Transf. 2022;137:106243.
[56] Shahzad F, Jamshed W, Safdar R, Mohd Nasir NAA, Eid MR, Alanazi MM, et al. Thermal valuation and entropy inspection of second-grade nanoscale fluid flow over a stretching surface by applying Koo–Kleinstreuer–Li relation. Nanotechnol Rev. 2022;11:2061–77.
[57] Jamshed W, Eid MR, Safdar R, Pasha AA, Mohamed Isa SSP, Adil M, et al. Solar energy optimization in solar-HVAC using Sutterby hybrid nanofluid with Smoluchowski temperature conditions: a solar thermal application. Sci Rep. 2022;12:11484.
[58] Akgül EK, Akgül A, Jamshed W, Rehman Z, Nisar KS, Alqahtani MS, et al. Analysis of respiratory mechanics models with different kernels. Open Phys. 2022;20:609–15.
[59] Jamshed W, Safdar R, Rehman Z, Lashin MMA, Ehab M, Moussa M, et al. Computational technique of thermal comparative examination of Cu and Au nanoparticles suspended in sodium alginate as Sutterby nanofluid *via* extending PTSC surface. J Appl Biomater & Funct Mater. 2022;1–20. doi: 10.1177/22808000221104004.
[60] Dhange M, Sankad G, Safdar R, Jamshed W, Eid MR, Bhujakkanavar U, et al. A mathematical model of blood flow in a stenosed artery with post-stenotic dilatation and a forced field. PLoS One. 2022;17(7):e0266727.
[61] Akram M, Jamshed W, Goud BS, Pasha AA, Sajid T, Rahman MM, et al. Irregular heat source impact on Carreau nanofluid flowing *via* exponential expanding cylinder: A thermal case study. Case Stud Therm Eng. 2022;36:102190.
[62] Shahzad F, Jamshed W, Ahmad A, Safdar R, Alam MM, Ullah I. Efficiency evaluation of solar water-pump using nanofluids in parabolic trough solar collector: 2nd order convergent approach. Waves Random Complex Media. 2022. doi: 10.1080/17455030.2022.2083265.
[63] Hussain SM, Jamshed W, Safdar R, Shahzad F, Mohd Nasir NAA, Ullah I. Chemical reaction and thermal characteristiecs of Maxwell nanofluid flow-through solar collector as a potential solar energy cooling application: A modified Buongiorno's model. Energy Environ. 2022;1–29. doi: 10.1177/0958305X221088113.
[64] Khan NS, Gul T, Islam S, Khan A, Shah Z. Brownian motion and thermophoresis effects on MHD mixed convective thin film

second-grade nanofluid flow with Hall effect and heat transfer past a stretching sheet. J Nanofluids. October 2017;6(5):812–29.
[65] Khan NS, Gul T, Islam S, Khan W. Thermophoresis and thermal radiation with heat and mass transfer in a magnetohydrodynamic thin-film second-grade fluid of variable properties past a stretching sheet. Eur Phys J Plus. 2017;132(1):1–20.
[66] Khan NS, Gul T, Islam S, Khan I, Alqahtani AM, Alshomrani AS. Magnetohydrodynamic nanoliquid thin film sprayed on a stretching cylinder with heat transfer. Appl Sci. 2017;7(3):271.
[67] Khan NS, Islam S, Gul T, Khan I, Khan W, Ali L. Thin film flow of a second grade fluid in a porous medium past a stretching sheet with heat transfer. Alex Eng J. June 2018;57(2):1019–31.
[68] Zuhra S, Khan NS, Islam S, Nawaz R. Complexiton solutions for complex KdV equation by optimal homotopy asymptotic method. Filomat. 2019;33(19):6195–211.